Research on Engineering Structures & Materials
www.jresm.org
Research Group

Research Article

Exploring the limits of flexural FRP strengthening in shear dominated reinforced concrete T beams

Yahia Taguia [*,1,a], Youcef Si Youcef [2,b], Sofiane Amziane [3,c]

[1]*Université des Sciences et de la Technologie Houari Boumediene, Algeria*
[2]*Ecole Polytechnique d'Architecture et d'Urbanisme, Algeria*
[3]*Clermont Université, Université Blaise Pascal, Institut Pascal, France*

Article Info

Article History:

Received 16 Jul 2026
Accepted 04 Oct 2026

Keywords:

RC beam;
CFRP;
GFRP;
Shear;
NSM;
Flexural;
Strengthening;
T-Beams

Abstract

The greatest challenge in strengthening deep reinforced concrete beams is overcoming brittle shear failure. Premature shear failure limits reliable flexural strengthening by preventing the full structural capacity of FRP reinforcement from being mobilized. To address this limitation, 36 RC T-beams with low shear span-to-depth ratios (a/d < 2.5), including under- and over-reinforced sections, were experimentally investigated. The beams were strengthened using externally bonded CFRP and bidirectional E-glass woven roving GFRP composites, the latter systematically evaluated as an economical strengthening alternative. An innovative NSM technique employing epoxy-impregnated rolled FRP sheets inserted into pre-cut grooves, acting similarly to conventional NSM FRP bars, was also developed. The experimental results showed that the effectiveness of FRP strengthening depended strongly on the reinforcement configuration and the governing failure mechanism. While selected configurations produced significant improvements in load-carrying capacity, ductility, and energy absorption, the tested beams predominantly exhibited diagonal cracking and brittle shear-dominated failure, which limited the full utilization of the FRP reinforcement. Across the four experimental series, the investigated FRP configurations produced a maximum 49.01% increase in load-carrying capacity, achieved with the U ±45° configuration, demonstrating the effectiveness of inclined FRP reinforcement in intercepting shear cracks and improving stress transfer. In terms of ductility, the configuration combining longitudinal reinforcement for the opening with 45° cross reinforcement exhibited the most pronounced improvement, with a 220.7% increase in energy-based ductility relative to the control beam. These findings demonstrate that, although FRP strengthening can substantially enhance the structural response of deep RC T-beams, shear remains a critical limiting mechanism. Integrated flexural shear strengthening is therefore essential to fully exploit the capacity of FRP systems in shear-dominated deep RC T-beams.

© 2026 MIM Research Group. All rights reserved.

1. Introduction

Several damage factors have given rise to the concept of strengthening through jacketing, which can be defined as a strengthening technique aimed at restoring or enhancing the structural performance of an element, based on a thorough understanding of its actual mechanical behavior, particularly in cases where the element is damaged or at risk of reaching a critical state. The progressive degradation of reinforced concrete structures has become a concerning reality, highlighting security vulnerabilities that require increased attention in the field of construction and public works [3]. This highlights the need to address the substantial human and material losses, which are often exacerbated by the inadequate dynamic performance of structures from the outset

*Corresponding author: t.yahia1992@gmail.com
[a]orcid.org/0009-0007-0563-4298; [b]orcid.org/0000-0002-6960-0798; [c]orcid.org/0000-0003-2339-3962
DOI: http://dx.doi.org/10.17515/resm2026-1900st0716rs

[4]. This issue is especially critical in regions prone to seismic activity and severe environmental conditions. In light of these challenges, it is essential to design and construct structures that can withstand seismic forces while mitigating the inherent degradation mechanisms of construction materials. As a result, the strengthening and rehabilitation of existing structures have become a strategic priority to safeguard both human lives and property. Currently, there exists a well-established body of research dedicated to the strengthening and repair of reinforced concrete structures, with the aim of developing techniques that restore their mechanical and energy-related performance [6]. Increasing attention is being directed toward the modernization of existing structures, with a particular emphasis on identifying alternative solutions to extend the service life of constructions that are at risk of failure. As highlighted by [10], a comprehensive diagnostic process, including the classification of the structural condition and assessment of damage severity, is essential to guide the selection of appropriate reinforcement strategies. The primary objective is to recover or enhance the structural system's performance and durability [11,12]. Numerous reinforcement techniques have been developed through experimental studies and subsequently implemented in practice to validate their real-world effectiveness.

Since the 1980s, numerous studies have investigated the potential of FRPs to enhance the load-bearing capacity of bridge piers and to control concrete compression through effective confinement, as highlighted in the works of [12] and [11]. According to the existing literature, FRP's have helped mitigate certain risks as they offer increased strength [5], ductility [7], and flexibility [13] at the engineer's disposal. Furthermore, several methods of applying these FRPs have been examined, both in real cases and through detailed studies. The simplicity of execution makes this technique widely adopted, for example, NSM systems have proven to be an effective and innovative technique for shear strengthening of shear-deficient reinforced concrete T-beams [14], and strongly used in safe smart sensing technologies that substantially enhance the understanding, detection, and prevention of FRP debonding failures in RC beams. An experimental investigation into the shear strengthening of reinforced concrete beams using basalt fiber-reinforced polymer (BFRP) strips was conducted by [16]. The study involved 18 reinforced concrete beams (150 mm × 250 mm × 2000 mm) with varying configurations in terms of fiber orientation, BFRP strip length, and wrapping schemes. Both experimental and analytical results demonstrated that full-section wrapping was the most effective technique for restoring and enhancing structural strength. Recent studies have increasingly focused on structural strengthening strategies [17-21] particularly through the application of fiber-reinforced polymer (FRP) composites. These materials have exhibited substantial potential in improving the mechanical performance of reinforced concrete elements [22]. FRP composites offer numerous advantages, including high tensile strength [23], lightweight characteristics [24], superior corrosion resistance [25,26], and enhanced confinement capabilities [27], which contribute to increased structural integrity and resistance to deformation and chemical deterioration[8,19]. Modern reinforcement techniques, particularly those involving carbon fiber-reinforced polymers (CFRP) and glass fiber-reinforced polymers (GFRP), have demonstrated significant potential in enhancing the load-bearing capacity of reinforced concrete (RC) elements [28,29]. These materials contribute to reducing crack formation and improving both flexural and shear resistance. This research falls within the scope of sustainable structural rehabilitation. Most FRP based strengthening strategies primarily aim to enhance flexural performance [30], particularly in regions subjected to high bending moments, especially the NSM systems[33]. Recently, the Side Near-Surface Mounted (S-NSM) technique has emerged as a promising variation of the NSM approach, in which FRP reinforcement is embedded in grooves cut along the side faces of the member. This technique offers improved ultimate load behavior [34], enhanced protection against premature debonding, decreased deflection, and better stress transfer compared to conventional externally bonded systems[36]. Recent destructive earthquakes have repeatedly demonstrated the vulnerability of existing reinforced concrete (RC) structures [37] and the critical need for effective structural assessment [38], rehabilitation, and strengthening. Major seismic events, including the 2019 Durrës earthquakes in Albania and the devastating 6 February 2023 Kahramanmaraş earthquake sequence in Türkiye, have revealed the consequences of inadequate seismic detailing, insufficient structural capacity, poor material quality, and other structural deficiencies, resulting in extensive damage and collapse [39]. These observations emphasize the importance of strengthening vulnerable RC members to improve structural safety

[40], deformation capacity, and seismic resilience. Seismic events can impose severe cyclic and lateral demands on existing RC structures, particularly on members with inadequate shear resistance or insufficient detailing [41]. Shear-critical members are of particular concern because shear failure is generally brittle and may occur with limited warning, potentially leading to a rapid loss of load-carrying capacity and severe structural damage. Consequently, the development of efficient strengthening techniques capable of enhancing both strength and deformation capacity is essential for improving the seismic resilience of existing RC structures. FRP composites offer attractive rehabilitation solutions owing to their high strength-to-weight ratio, corrosion resistance, and ease of application. However, in certain structural configurations, such as short-span beams or members with low shear span-to-depth ratios ($a/d < 2.5$), structural behavior is often governed by shear rather than flexure. In these cases, conventional externally bonded FRP systems and flexural strengthening alone may be insufficient to prevent brittle shear-dominated failure. This limitation highlights the need for strengthening strategies specifically designed to enhance shear resistance, promote effective shear-crack interception and stress redistribution, and improve deformation capacity. Accordingly, the present study experimentally investigates different CFRP and GFRP strengthening configurations for shear-dominated RC T-beams, with particular emphasis on the effectiveness of inclined U-shaped reinforcement, E-glass woven roving, and an NSM system based on rolled FRP sheets. Although Near Surface Mounted (NSM) FRP systems have been increasingly adopted to improve bond efficiency and ductility [32] [42], their application has also predominantly focused on flexural enhancement [43], with limited consideration of flexure shear interaction. This highlights a critical gap in current strengthening practices, particularly where design assumptions do not adequately address shear mechanisms and combined failure modes.

In addition to experimental investigations, analytical and numerical approaches have been increasingly employed to quantify the contribution of FRP strengthening to the structural response of reinforced concrete members. Such studies provide valuable insight into the interaction between FRP reinforcement, concrete, and internal steel reinforcement, while enabling the prediction of strength and deformation response under different strengthening configurations [44] [45]. Nevertheless, experimental validation remains essential, particularly for shear-dominated members where crack development, stress redistribution, anchorage, and failure mechanisms can significantly influence the effectiveness of FRP strengthening. Despite extensive research on FRP-strengthened RC members, the quantitative behavior of shear-dominated T-shaped deep beams remains insufficiently documented, particularly across different reinforcement ratios and strengthening conditions. Most existing studies primarily address flexural strengthening or conventional beam configurations, providing limited comparative evidence on the interaction between reinforcement ratio, FRP type, shear-governed failure, strength, and ductility. The present study addresses this gap through a systematic experimental investigation of CFRP- and GFRP-strengthened T-beams under under- and over-reinforced conditions. Beyond demonstrating the effectiveness of FRP, the study establishes quantitative relationships between strengthening configuration, load-carrying capacity, and ductility, providing practical performance indicators for engineering selection. The results offer a clearer basis for strengthening decisions while establishing an experimental reference for researchers developing analytical and numerical models of shear-critical RC members. A total of 36 beams were tested under four-point loading and strengthened using CFRP, GFRP jacketing, and Near-Surface Mounted (NSM) techniques. Although the applied systems enhanced load capacity and ductility [46], most beams exhibited premature shear failure, indicating that flexural strengthening alone is insufficient in such conditions. The results highlight the need for combined flexural and shear reinforcement to achieve reliable and ductile structural performance.

2. Experimental Work

The experimental study of reinforced concrete T-beams strengthened with composite materials aims to assess their structural performance under monotonic loading. This research focuses on evaluating the effectiveness of various strengthening techniques, particularly in enhancing the post-elastic behavior of beams. The study involves reinforcing T-shaped beams as presented in Fig.

1, with carbon and glass fiber fabrics (CFRP and GFRP respectively), applying different configurations, and analyzing their Force-Displacement response. A total of (36) reinforced concrete T-beams, with cross-sectional dimensions as detailed in Fig. 1, were tested.

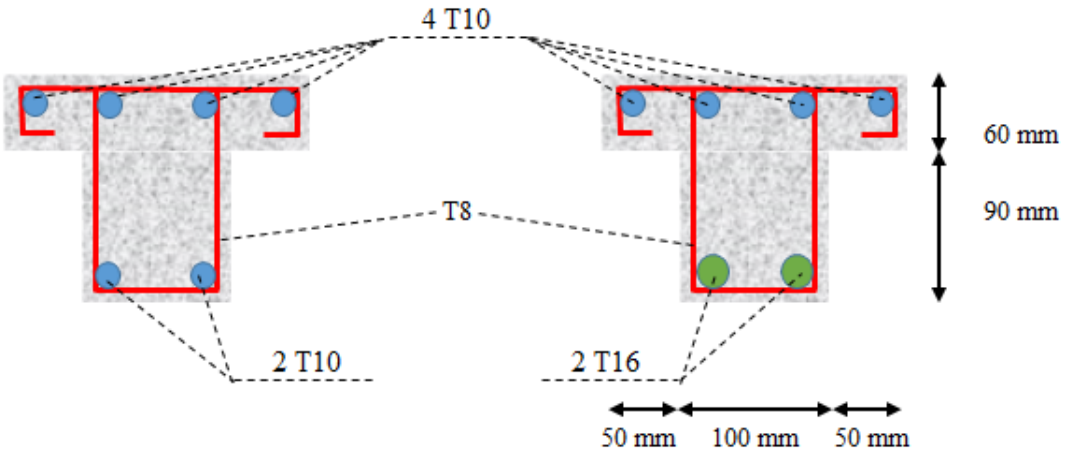


Fig. 1. Tested sections

Key experimental parameters include the internal reinforcement ratio Table 1, composite material type, reinforcement configuration, and a constant shear span-to-effective depth ratio (a/d). Beam length is (1100 mm, with a shear span (a=300 mm), and effective depth (d=127 mm) for under-reinforced beams and (d=124 mm) for over-reinforced beams, resulting in (a/d = 2.36) for under-reinforced beams and (a/d = 2.42) for over-reinforced beams. Special attention is given to low-strength concrete to assess the real behavior of deteriorated or poorly constructed beams. The study examines failure modes, the influence of different fiber fabric types (carbon, glass), reinforcement configurations, and post-elastic behavior in terms of stiffness, ductility, ultimate load, and energy absorption. Tests were conducted using an MTS Criterion 45 universal testing machine (maximum load capacity of 300 kN) to ensure precise load application and displacement measurement. The findings provide critical insights into the efficiency of composite reinforcements and their impact on the overall behavior of T-beams, helping to optimize their use in real-world structural applications.

Table 1. Steel reinforcement ratios for all configurations

Steel reinforcement ratios (%)		2.13	2.29
Configurations	Control beam	UB0	OB 0
	Carbone reinforcement	UCB1, UCB2, UCB3 UCB4, UCB5 UCB6, UCB7	OCB1, OCB2, OCB3 OCB4, OCB5 OCB6, OCB7
	Glass reinforcement	UGB1, UGB2, UGB3 UGB4, UGB5, UGB6 UGB7, UGB8	OGB1, OGB2, OGB3 OGB4, OGB5, OGB6 OGB7, OGB8

2.1 Description and Characterization of the Materials Introduced

The study focuses on characterizing the materials used in reinforced concrete T-beams strengthened with CFRP and GFRP, tested under four points bending system.

2.1.1 Characterization Program

The concrete mix used in this study was prepared following standard practice to ensure uniformity and repeatability, with detailed material characteristics summarized in Table 2. The concrete mix proportions also reported in Table 3. The mechanical properties of the steel reinforcement were determined through monotonic tensile testing in accordance with ASTM E8/E8M, as reported in Table 4.

Table 2. Concrete mix details

Parameter	Description / Value
Target compressive strength	12.43 MPa
Cement type	Ordinary Portland Cement (CEM II/A-P 42.5 N)
Water-cement ratio (w/c)	0.84
Fine aggregates	Natural fine sand and washed coarse sand (0/4), standard grading
Coarse aggregates	Crushed gravel (5/15), low hardness, irregular shapes
Admixtures	None
Purpose of mix	Low-strength baseline to evaluate FRP strengthening efficiency
Batch usage	Each batch used to cast 2 T-beams and 2 prismatic specimens (150×150×150 mm^3)
Standards followed	NF EN 12390-3
Slump	14 cm
Reason for high w/c ratio	Achieve low strength suitable for deteriorated or poorly constructed beams
Mechanical performance consideration	Aggregates and absence of admixtures deliberately limit strength

Table 3. Concrete mix proportions

Constituent	Quantity (kg/m^3)
Cement	246
Fine sand	705.56
Coarse sand	213.03
Gravel	960.44
Water	179.4
Target compressive strength	12.43 MPa

Table 4. Properties of steel reinforcement

Reinforcement Type	Diameter (mm)	Young's Modulus E (GPa)	Yield Strength fy (MPa)	Role
T10	10	200	600	Longitudinal
T16	16	200	550	Longitudinal
T8	8	200	500	Transverse

2.1.2 Composite Materials

In this study, a unidirectional carbon fiber reinforced polymer (CFRP) fabric (Table 5), SikaWrap-230 C, was employed due to its high tensile strength and stiffness. For comparison, a bidirectional glass fiber fabric (GFRP, Woven Roving E300) was also used (Table 4). Both composite systems were bonded to the concrete substrate using Sikadur-330 epoxy resin, selected for its high adhesion capacity and effective stress transfer, in accordance with relevant application standards.

Table 5. Mechanical properties of the reinforcement fabrics

Property	SikaWrap-230 C	Sikadur-330	Woven Roving E300	CFRP Laminate
Fiber Orientation	0° (Unidirectional)	/	0°/90° (Bidirectional)	/
Tensile Strength (MPa)	4000	30	≥2000 N/75 mm	3500
Elastic Modulus (GPa)	230	4.5	/	225
Elongation at Break (%)	1.70	0.90	/	1.56
Thickness (mm)	0.129	/	1.2	0.129

Technical details were provided by Sika El Djazair SPA and Sarl SPPF Algeria. These materials and configurations form the basis for evaluating the structural improvements in reinforced concrete beams using FRP composites.

2.1.3 Design and Preparation of Specimens

T-shaped reinforced concrete beams were designed and tested under four-point bending, as illustrated in Fig. 2, to ensure a constant bending moment region and representative assessment of structural performance. This configuration is well suited for evaluating the behavior of reinforced concrete elements under flexural loading. Concrete proportions were determined using the Dreux–Gorisse method. Steel reinforcement cages were accurately assembled before casting; concrete was placed in layers with vibration, then cured under controlled humid conditions.

2.1.4 Reinforcement Preparation

Reinforcement steel bars were selected according to design requirements and available grades, then precisely cut to specified lengths using a bar cutter.

2.1.5 Surface Preparation and Reinforcement Application

Following a thorough inspection of the concrete surfaces, the areas designated for strengthening were carefully cleaned and mechanically roughened to remove loose particles and surface contaminants and to promote effective mechanical interlocking and epoxy adhesion. The CFRP and GFRP fabrics, as well as the NSM reinforcement systems, were subsequently installed in the prescribed orientations in accordance with the manufacturer's recommendations. Particular attention was given to the alignment, positioning, and continuity of the reinforcement to ensure proper stress transfer between the FRP system and the concrete substrate. The strengthened specimens were then maintained under the recommended curing conditions prior to testing.

2.2 Testing Machines Used

2.2.1 Flexural Testing

Based on a review of the literature, it was observed that most reinforced concrete elements tested are scaled in dimensions, either to study the size effect or due to limitations imposed by the testing machine's capacity. These constraints are typically defined by the machine's load capacity, the dimensions of the tested specimens, measurement precision, and the versatility to accommodate various operating conditions. The MTS Criterion Model 45 universal testing machine was used for our four-point bending tests. The MTS Criterion Model 45 is known for its high precision in measuring loads and displacements. It employs high-accuracy force and displacement sensors, enabling it to detect even the smallest variations, which is essential for our tests.

2.2.2 Compression Testing

Compressive strength was evaluated on (150×150×150 mm) concrete prisms using a (2000 kN) Lindqvist International hydraulic testing machine with AUTOCON control, ensuring reliable results.

2.2.3 Tensile Testing

Tensile tests on steel reinforcing bars (T10 and T16) were performed using an Instron SATEC machine. This latter provides high precision, flexibility for testing, and compliance with international standards.

2.2.4 Pull-Off Testing

Pull-off tests were conducted using a Proceq DY-216 device in accordance with ASTM C1583 to evaluate tensile bond strength, results are shown in Table 6.

Table 6. Pull-Off bond strength results

Specimen	Bond Strength 1 (MPa)	Bond Strength 2 (MPa)	Bond Strength 3 (MPa)	Average Bond Strength (MPa)
UCB2	0.94	1.55	1.15	1.21
UCB5	0.71	0	1.23	0.64
OCB5	0.53	1.57	0	0.70
UGB2	1.84	2.08	1.8	1.91
UGB5	0.74	1.49	1.48	1.24
OGB7	1.75	1.38	1.43	1.52

3. Design of Test Specimens

A total of 36 T-shaped reinforced concrete beams were fabricated at laboratory scale using low-strength concrete with a measured compressive strength of 12.43 MPa. This relatively low-strength substrate provided a mechanically weak condition for evaluating the effectiveness and limitations of the applied FRP strengthening systems. Beams were cast in accurately dimensioned molds, cured under controlled conditions, and provided with transverse stirrups at (150 mm) spacing to ensure stable behavior. Concrete surfaces were carefully prepared prior to strengthening, and external CFRP/GFRP reinforcements were applied over (820 mm) in various configurations to evaluate flexural strengthening effectiveness.

3.1 Beam Series and Strengthening Objectives

- The UCB (Under-reinforced Carbon Fiber Beam) was reinforced with two T10 bars in the tension zone and CFRP applied with different configurations.
- The OCB (Over-reinforced Carbon Fiber Beam) had two T16 bars in the tension zone and CFRP applied either to the bottom of the flange or on the lateral webs in a U-shape.
- Similarly, the UGB (Under-reinforced Glass Fiber Beam) was reinforced with two T10 bars and GFRP applied employed with distinct setup patterns.
- Lastly, the OGB (Over-reinforced Glass Fiber Beam) incorporated two T16 bars in the tension zone with GFRP installed in different reinforcement schemes.

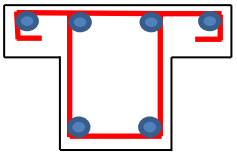
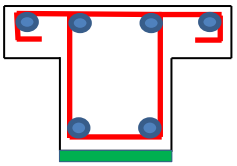
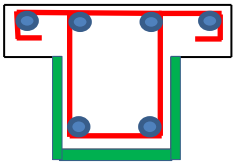
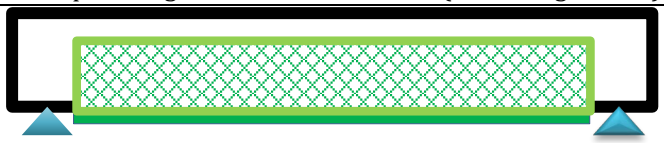
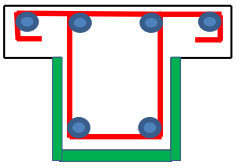
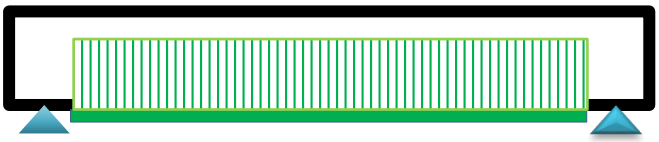
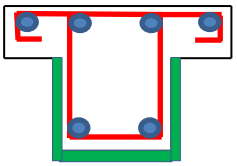
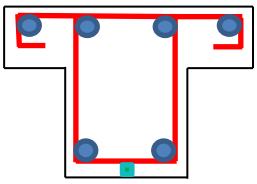
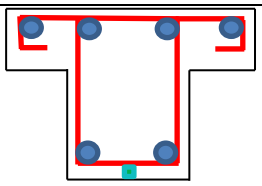
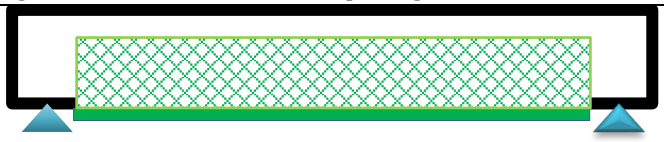
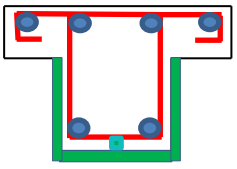
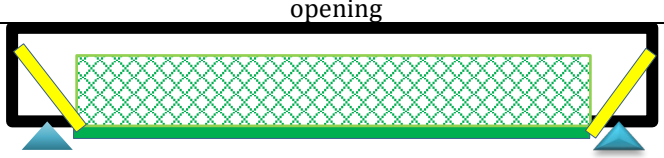
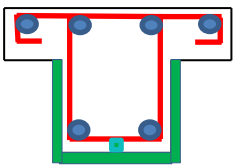
3.2 Control Beams

To compare the performance of strengthened beams, six unreinforced control beams were fabricated and tested without any external composite reinforcement. These beams serve as a baseline to assess the efficiency of the various reinforcement configurations.

3.3 Testing and Performance Evaluation

The beam specimens were tested under four-point bending with monotonic static loading. while load and deflection were continuously recorded to assess structural response and quantify the effectiveness of external strengthening by comparison with reference beams, enabling identification of the most efficient flexural strengthening configurations Table 7.

Table 7. The testing program configurations

	Configuration	Section
UB 0	 Reference beam	
UCB 1	 Longitudinal reinforcement on the bottom face	
UCB 2	 U shaped Longitudinal reinforcement (U-0 configuration)	
UCB 3	 U-shaped ±45° cross reinforcement	
UCB 4	 U-shaped longitudinal reinforcement (0°/90° configuration)	
UCB 5	 Longitudinal reinforcement for opening (reservation)	
UCB 6	 Longitudinal reinforcement for opening with 45° end anchorage	
UCB 7	 U-shaped ±45° cross reinforcement + Longitudinal reinforcement for opening	
UCB 8	 U-shaped ±45° cross reinforcement + Longitudinal reinforcement for opening with 45° end anchorage	

The RC beam specimens were simply supported with a span of 900 mm and subjected to four-point bending, with the two loading points separated by 300 mm. Displacement was precisely measured using the integrated actuator sensor of the testing frame, ensuring accurate monitoring of mid-span deflections. Fig. 2 illustrates the experimental setup, showing the positioning of the beam and load application points. The experimental program was designed to investigate the effectiveness of FRP strengthening in shear-critical RC T-beams while considering the influence of the longitudinal reinforcement condition. Two levels of longitudinal reinforcement were adopted, corresponding to reinforcement ratios of 2.13% and 2.29%. The classification of the specimens as under-reinforced or over-reinforced was established by comparing the actual longitudinal reinforcement ratio with the corresponding balanced reinforcement ratio, rather than by the numerical reinforcement ratio alone. This approach ensured that the two groups represented distinct flexural reinforcement conditions.

A low shear span-to-effective depth ratio (a/d) was maintained for all specimens to establish a consistent shear-critical structural framework. Within this framework, the experimental matrix varied the FRP material and strengthening configuration while maintaining the principal geometric and loading parameters. This organization enabled the effects of the longitudinal reinforcement condition, FRP type, and strengthening configuration to be examined systematically. The experimental design therefore combines two complementary aspects of structural behavior: the longitudinal reinforcement ratio defines the flexural condition of the section, while the low (a/d) ratio promotes shear-dominated behavior. The resulting matrix provides a controlled basis for examining how FRP strengthening modifies strength, deformation, stiffness, and failure mechanisms under different reinforcement conditions.

4. Responses and Discussions

4.1 Response of Control Beams

UB0 and OB0 were tested under static monotonic flexural loading at 0.02 mm/s using a 300 kN force and displacement sensor (displacement limited to 45 mm). Photographs were taken throughout, and data analyzed. Some beams were reclassified (UCB8/OCB8) due to the absence of reinforcement; UB0 and OB0 failed prematurely due to shear.

UB0, an under-reinforced beam, exhibited a typical three-phase behavior. In the elastic phase, the concrete remained uncracked up to (34.57 kN). The cracked phase followed, during which deformations increased, stiffness decreased, and plastic deformation of the steel progressed up to the peak load. In the failure phase, deformation increased significantly, and the beam reached a peak load of (55.97 kN) with a maximum displacement of (7.92 mm). Failure was governed by shear mechanisms, followed by crushing of the concrete in the compression zone, with limited ductility. According to, this failure mode is sudden and occurs at relatively low deflections.

OB0, an over-reinforced beam, demonstrated similar three-phase behavior. In the elastic phase, the beam remained linear until the first crack appeared at (46.3 kN), maintaining high stiffness due to concrete compression and steel tension. In the cracked phase, shear-induced cracks in the tensile zone reduced stiffness as stress redistributed between concrete and reinforcement. Steel plastification occurred, allowing the beam to carry higher loads despite stiffness degradation. In the failure phase, OB0 reached a peak load of (70.58 kN) and a maximum displacement of (6.90 mm) before failing in a brittle manner. Failure resulted from tensile steel plastification and concrete crushing in the flange. The brittle nature of OB0's failure was due to its over-reinforced condition, which limited deformation before collapse. Shear-compression failure was observed as diagonal cracks propagated into the compression zone, ultimately leading to concrete crushing.

4.1.1 Shear Compression Failure Analysis

Shear-compression failure in reinforced concrete T-beams is closely linked to the shear span-to-depth ratio (a/d), particularly in the range of $1 \leq a/d \leq 2.5$, where beams are classified as deep and susceptible to this failure mode. In such cases, diagonal cracks initiate in the tensile zone near supports or loading points and propagate directly into the compressed zone, bypassing the formation of secondary cracks typically associated with flexural failure. This crack pattern

concentrates stress in the compression zone, often leading to premature crushing of the concrete before the beam can develop its full flexural capacity. The shear capacity in this regime is highly dependent on the (a/d) ratio, and in this study, it was significantly compromised by the poor quality of concrete, which limited the contribution of externally bonded CFRP and GFRP reinforcement. While arching action an internal load-transfer mechanism in deep beams can enhance shear resistance by mobilizing compressive struts and reducing tensile stress, its effectiveness was diminished by the low compressive strength of the concrete. As a result, the beams exhibited a brittle failure mechanism Fig. 2, marked by diagonal crack widening and crushing in the compression zone, ultimately restricting the composite strengthening systems from reaching their full potential.



Fig. 2. Failure modes for the UCB series

4.2 Responses of Beams Reinforced with Different Configurations

4.2.1 Load Carrying Capacity and Deflection Responses of Beam Specimens

- UCB Series:

Seven RC beams (2T10 steel in tension) were strengthened with unidirectional CFRP sheets; the following Fig. 3 shows specimens UCB1 through UCB7.

UCB 1, reinforced with a CFRP sheet at 0° on the web's lower surface, failed due to compression and shear, reaching (63.6 kN, 13.63% gain) with a deflection of 7.11 mm, showing minimal CFRP contribution. UCB 2, with a U-shaped CFRP at 0°, slightly improved strength (57.79 kN, 3.25% gain) but experienced failure governed by a shear-compression mechanism. UCB 3, with ±45° U-shaped CFRP, showed the highest strength gain (83.06 kN, 48.4%) and improved shear resistance with a

deflection of 9.8 mm. UCB 4, with 0° longitudinal and 90° transverse CFRP, reached (73.24 kN, 30.85% gain) but had premature shear failure due to stiffness mismatch with no delamination observed. UCB 5, strengthened with a grooved 10 cm-wide CFRP strip, unexpectedly decreased in capacity (52.34 kN, 6.48% reduction), failing in brittle shear. UCB 6, using grooved CFRP with 45° anchorage, enhanced shear resistance (73.75 kN, 31.76% gain) with reduced diagonal cracking. UCB 7, the specimen was strengthened using a grooved NSM reservation without any end anchorage, in combination with a ±45° U-shaped CFRP configuration. The CFRP sheets applied on the bottom and lateral faces were oriented at ±45° to enhance the diagonal shear resistance by intercepting principal tensile crack paths. Although no mechanical or bonded anchorage was introduced at the groove ends, the ±45° orientation of the U-shaped CFRP inherently provided a form of indirect anchorage, as the fibers crossed the shear-critical zone diagonally. combining grooved and ±45° U-shaped CFRP, improved ductility and crack control, reaching (62.49 kN, 11.64% gain). The ±45° CFRP cross reinforcement proved most effective in reducing shear cracks and stress concentrations, significantly improving durability and ductility, while composite bar anchorage at 45° acted as an efficient shear reinforcement mechanism; responses are shown in.

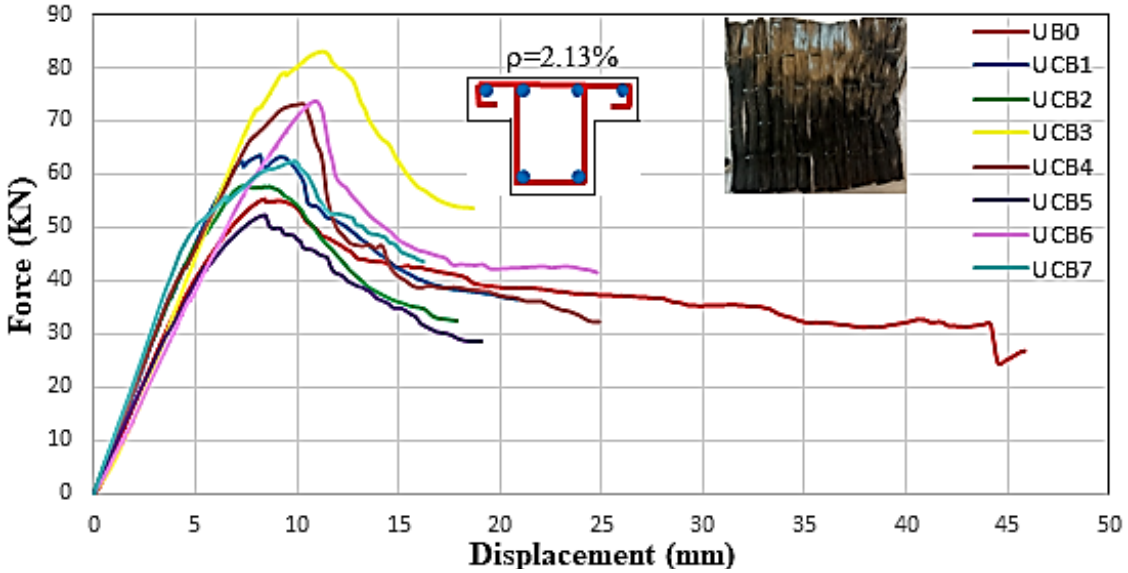


Fig. 3. Load-displacement response curve for UCB



Fig. 4. Beam crushed by Shear forces

- OCB Series:

The OCB series studied seven RC beams with two T16 tensile steel bars, strengthened using unidirectional CFRP fabrics in various configurations. The results Fig. 5 show that OCB 3, with ±45° CFRP reinforcement, exhibited the highest performance, reaching a peak load of 105.23 kN (49.09% increase over OB0 and 88% over UB0) with a displacement of 10.18 mm. This configuration effectively delayed shear cracks and improved structural integrity. OCB 1 and OCB 2, both with longitudinal CFRP reinforcement, achieved similar strength gains of approximately 19% over OB0, with peak loads of 83.81 kN and 84.32 kN, respectively. However, these configurations were limited by premature failure due to compression-shear interaction. OCB 4, featuring a 0°/90° U-shaped reinforcement, showed a moderate improvement, with a peak load of 89.81 kN (22.99% over OB0, 55.09% over UB0) and a displacement of 8.95 mm, but failed to significantly outperform OCB 2. OCB 5 demonstrated a lower performance, with a peak load of 62.78 kN (11.04% lower than OB0) and minimal CFRP contribution due to dominant shear stresses. OCB 6 and OCB 7, incorporating composite bars with 45° anchorage, reached peak loads of 74.64 kN and 71.2 kN, respectively, but their gains were lower than expected due to the limited shear resistance of the concrete. The study concludes that ±45° CFRP reinforcement (OCB 3) is the most effective configuration for increasing load-bearing capacity, crack control, and ductility. However, the effectiveness of CFRP reinforcement is strongly influenced by the concrete's compressive strength, as observed in OCB 4 and OCB 6, where potential gains were restricted by shear stress concentrations and low concrete strength; Furthermore, the failure mode significantly influences the overall ductility, as it dictates the element's capacity to undergo inelastic deformations and dissipate energy before failure.

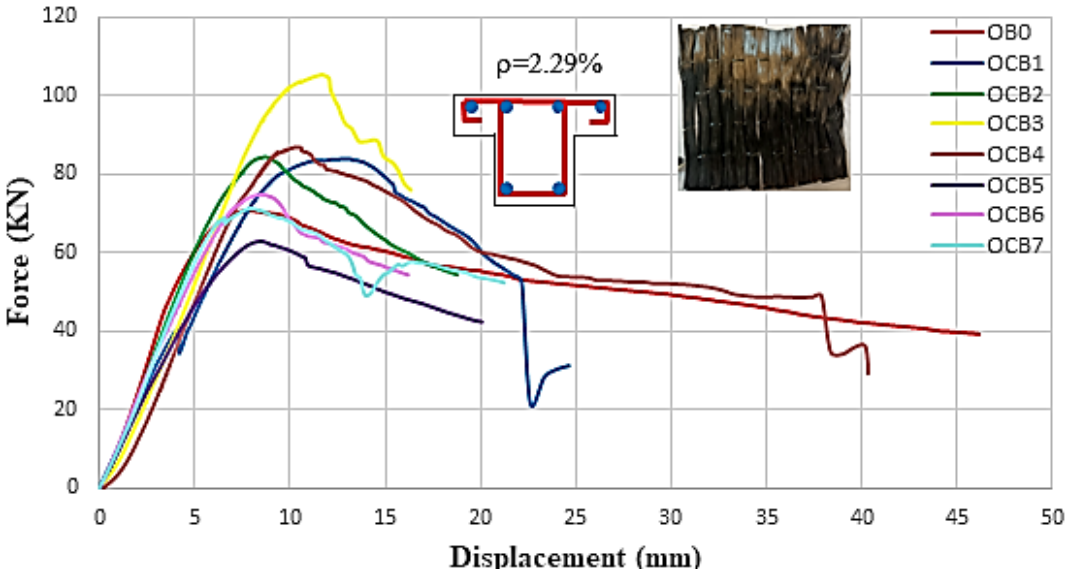


Fig. 5. Load-displacement response curve for OCB

- UGB Series:

This study investigates eight RC beams initially reinforced with 2T10 steel bars in tension and retrofitted with bidirectional GFRP fabrics in various configurations to evaluate effects on stiffness, ultimate load, and ductility.

The results reveal significant variation in performance depending on the layout and orientation of the GFRP Fig. 6. Beam UGB1 achieved a 14.92% increase in peak load compared to the control (UB0), yet failure was governed by premature shear-compression rupture, preventing full exploitation of the reinforcement. A similar brittle failure limited UGB2's gain to only 1.66%. In contrast, UGB3, with a U-shaped 45° fiber layout, demonstrated a remarkable 35.38% improvement, attributed to enhanced transverse confinement and delayed shear crack propagation. UGB4, using a 0°/90° U-wrap, reached a comparable gain (35.71%), though no substantial advantage was observed over simpler configurations. UGB5 exhibited the weakest performance, with a 9.45% decrease in load capacity due to the ineffective engagement of the grooved GFRP bar, which showed detachment and no deformation. UGB6 and UGB7, despite

different anchor schemes, yielded similar moderate gains (9.85% and 8.92%, respectively), again limited by early shear failure and poor concrete crushing resistance. Finally, UGB8, combining an anchored bar and a 45° U-wrap, achieved the highest performance (82.09 kN, +46.86%), matching the best CFRP-reinforced beams UCB3, with minimal delamination observed post-failure. These findings underline the critical importance of reinforcement orientation, anchorage strategy, and shear mitigation in optimizing the contribution of GFRP systems to concrete beam strengthening.

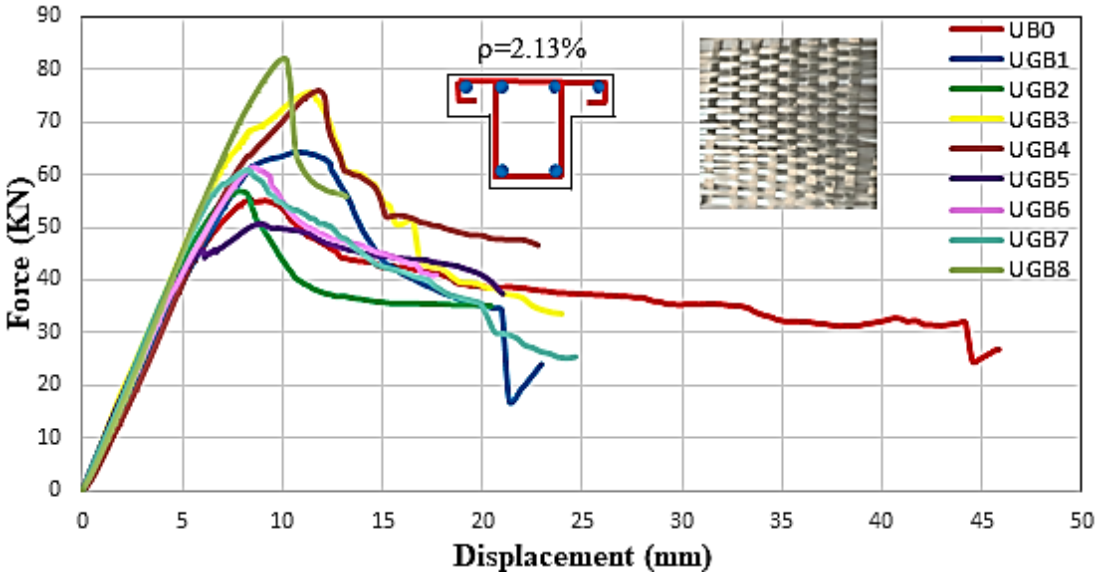


Fig. 6. Load-displacement response curve for UGB

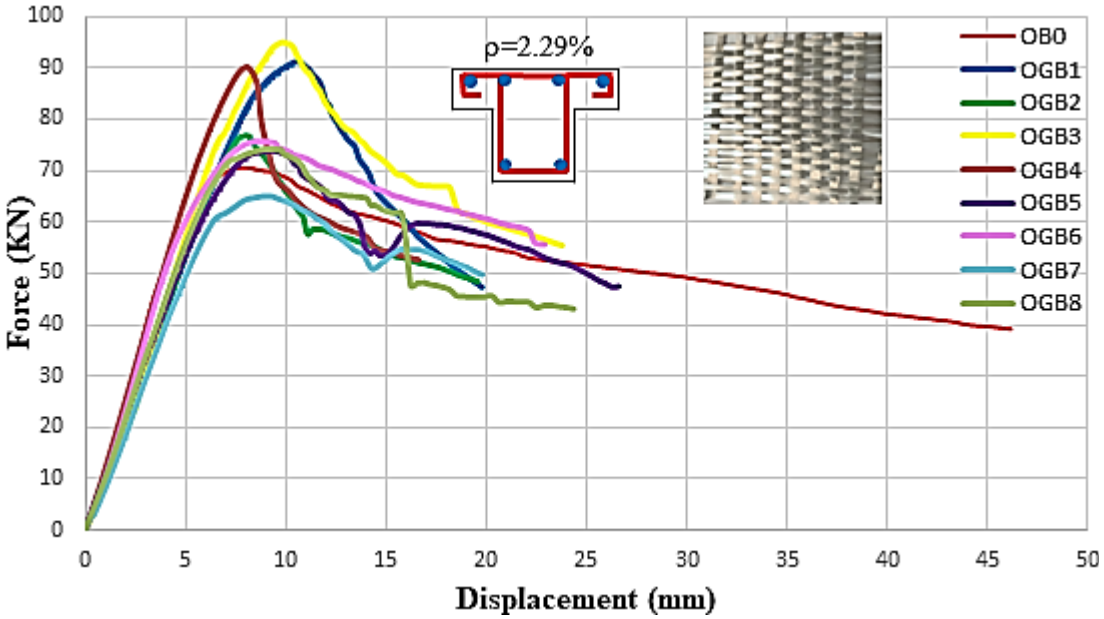


Fig. 7. Load-displacement response curve for OGB

- OGB Series:

The OGB series studied eight RC beams initially reinforced with 2T16 steel bars in tension and subsequently retrofitted with custom-cut bidirectional GFRP fabrics applied in diverse reinforcement configurations.

Test results for each beam are analyzed individually, allowing direct comparison of structural performance across configurations Fig. 7. For instance, OGB1 exhibited a 29.29% increase in peak load (91.26 kN) and a (33.9 %) increase in displacement over the non-strengthened OB0 beam and 63.05% over UB0, with shear-compression failure dominating and the GFRP remaining intact, indicating premature failure due to concrete limitations and an (a/d) ratio below (2.5), rather than reinforcement deficiency. OGB2 showed only an 8.9% improvement (76.86 kN) and similar shear-

compression behavior, again with no damage to the GFRP. In contrast, OGB3 demonstrated significant enhancement (94.99 kN, 34.59%), attributed to the optimized 45° fiber orientation and U-shaped confinement, which delayed shear crack propagation. OGB4 also maintained GFRP integrity while reaching 90.18 kN (27.77%), similar to OCB4. OGB5 yielded the lowest gain (73.88 kN, 4.68%) but high ductility, with the GFRP bar disengaging from its groove due to shear domination. OGB6 and OGB7 recorded modest to no improvements (75.69 kN, 7.24%; 65.03 kN, 7.86%), limited again by premature shear-compression failure. Finally, OGB8 combined the features of OGB6 and OGB7, reaching 74.21 kN (5.15%) with minimal GFRP damage but similarly governed by brittle shear failure. These findings highlight the critical role of fiber orientation, anchorage method, and the interaction between reinforcement and shear-compression effects in determining the effectiveness of GFRP strengthening systems. Normalized strength and deflection (%) for all series, showing the relative performance of each beam compared to its reference are as follow Table 8 and Table 9.

Table 8. Normalized strength and deflection for UCB and OCB series (%)

	Configurations	Ultimate load (KN)	Deflection (mm)	Normalized strength (%)	Normalized deflection (%)
UB 0	Reference beam	55.97	7.93	100	100
UCB1	Longitudinal reinforcement on the bottom face	63.60	7.11	113.62	89.68
UCB2	Longitudinal reinforcement on the bottom face + lateral faces (U-0 configuration)	57.79	6.40	103.25	80.79
UCB3	45° cross reinforcement on the bottom face + lateral faces (U ±45 configuration)	83.06	9.80	148.40	123.59
UCB4	Longitudinal reinforcement on the bottom face + lateral faces at 90° (U 0/90 configuration)	73.24	8.88	130.84	112.09
UCB5	Longitudinal reinforcement for opening (reservation)	52.34	7.28	93.52	91.87
UCB6	Longitudinal reinforcement for opening with 45° end anchorage	73.75	9.50	131.75	119.90
UCB7	Longitudinal reinforcement for opening + 45° cross reinforcement (U configuration)	62.49	8.59	111.64	108.40
UCB8	Longitudinal reinforcement for opening with 45° end anchorage + 45° cross reinforcement (U configuration)	/	/	/	/
OB 0	Reference beam	70.58	6.90	100	100
OCB1	Longitudinal reinforcement on the bottom face	83.81	11.19	118.74	162.19
OCB2	Longitudinal reinforcement on the bottom face + lateral faces (U-0 configuration)	84.32	7.53	119.46	109.05
OCB3	45° cross reinforcement on the bottom face + lateral faces (U ±45 configuration)	105.23	10.18	149.09	147.57
OCB4	Longitudinal reinforcement on the bottom face + lateral faces at 90° (U 0/90 configuration)	86.81	8.96	122.98	129.77
OCB5	Longitudinal reinforcement for opening (reservation)	62.78	7.37	88.95	106.73
OCB6	Longitudinal reinforcement for opening with 45° end anchorage	74.64	7.49	105.75	108.58
OCB7	Longitudinal reinforcement for opening + 45° cross reinforcement (U configuration)	71.20	6.87	100.87	99.48
OCB8	Longitudinal reinforcement for opening with 45° end anchorage + 45° cross reinforcement (U configuration)	/	/	/	/

Table 9. Normalized strength and deflection for UGB and OGB series (%)

	Configurations	Ultimate load (KN)	Deflection (mm)	Normalized strength (%)	Normalized deflection (%)
UGB1	Longitudinal reinforcement on the bottom face	64.32	9.34	114.92	117.78
UGB2	Longitudinal reinforcement on the bottom face + lateral faces (U-0 configuration)	56.90	6.79	101.66	85.67
UGB3	45° cross reinforcement on the bottom face + lateral faces (U ±45 configuration)	75.77	9.90	135.38	124.92
UGB4	Longitudinal reinforcement on the bottom face + lateral faces at 90° (U 0/90 configuration)	75.96	10.25	135.72	129.29
UGB5	Longitudinal reinforcement for opening (reservation)	50.68	7.73	90.54	97.49
UGB6	Longitudinal reinforcement for opening with 45° end anchorage	61.48	7.42	109.85	93.66
UGB7	Longitudinal reinforcement for opening + 45° cross reinforcement (U configuration)	60.97	7.17	108.92	90.49
UGB8	Longitudinal reinforcement for opening with 45° end anchorage + 45° cross reinforcement (U configuration)	82.10	8.80	146.68	110.99
OGB1	Longitudinal reinforcement on the bottom face	91.26	9.24	129.30	133.90
OGB2	Longitudinal reinforcement on the bottom face + lateral faces (U-0 configuration)	76.86	6.98	108.90	101.15
OGB3	45° cross reinforcement on the bottom face + lateral faces (U ±45 configuration)	94.99	8.60	134.59	124.60
OGB4	Longitudinal reinforcement on the bottom face + lateral faces at 90° (U 0/90 configuration)	90.18	7.03	127.77	101.81
OGB5	Longitudinal reinforcement for opening (reservation)	73.89	8.09	104.68	117.23
OGB6	Longitudinal reinforcement for opening with 45° end anchorage	75.69	7.49	107.24	108.53
OGB7	Longitudinal reinforcement for opening + 45° cross reinforcement (U configuration)	65.03	7.99	92.13	115.77
OGB8	Longitudinal reinforcement for opening with 45° end anchorage + 45° cross reinforcement (U configuration)	74.22	8.21	105.15	118.97

4.2.2 Responses in Terms of Ductility

The ductility of RC beams strengthened with CFRP and GFRP composites was assessed using two methods:

- An energy-based approach, calculating the area under the load displacement curve to failure.
- A displacement ratio method, comparing ultimate displacement to the elastic limit displacement.

Results show moderate ductility improvements in strengthened beams; however, shear-dominated failures, caused by low concrete strength and a shear span to depth ratio below (2.5), limited fully plastic behavior. CFRP and GFRP reinforcements delayed failure and slightly enhanced energy absorption. The energy-based approach proved more sensitive to post-elastic behavior, whereas

the displacement ratio method underestimated ductility in sudden failures, highlighting the benefit of using both approaches for comprehensive assessment. The results of the four series are as follows:

- UCB Series:

The results revealed distinct trends across this group. The ductility behavior of the whole under-reinforced concrete beams strengthened with CFRP configurations was investigated through both energy-based (μ_E) and displacement-based (μ_Δ) indices Table 10. The unstrengthen control beam (UB0) exhibited a baseline energy ductility of 2.19 and displacement ductility of 1.50. Strengthened specimens (UCB1 to UCB7) showed varying improvements depending on the CFRP configuration. Among them, UCB7 recorded the highest ductility values, with (μ_E) = 7.01 corresponding to a 220.7% increase relative to UB0, along with a 109.7% increase in displacement ductility (μ_Δ) = 3.14, reflecting a substantial enhancement in energy dissipation and post-yield deformation capacity. Similarly, UCB4 and UCB6 showed high energy ductility (6.18 and 5.93, respectively) corresponding to 182.8% and 171.4% of increase, and relatively high displacement ductility (2.73 and 2.49) corresponding to 82.3% and 66.1% of increase respectively, suggesting that CFRP layouts can significantly increase structural ductility in the longitudinal direction. Conversely, beams such as UCB1 exhibited limited ductility gains of 8.5% in energy-based ductility and 3.8% in displacement-based ductility. UCB2 and UCB3 demonstrated more substantial gains, with UCB2 reaching 65% (μ_E = 3.61) and 30.0% (μ_Δ = 1.95), while UCB3 increased by 15.7% and 12%, respectively, which is likely due to limited composite action or stiffer reinforcement behavior. This variation highlights the influence of CFRP application configuration on ductility performance. Overall, the results confirm that optimized CFRP strengthening in under-reinforced beams can considerably enhance both energy absorption and deformation capacity, contributing to a more ductile failure mode and improved structural performance.

Table 10. Ductility for all UCB beams

Specimen	Max elastic load (KN)	Energy E_u	Energy E_y	Δ_u (mm)	Δ_y (mm)	μ_E	μ_Δ	μ_E Gain ratio	μ_Δ Gain ratio	Steel reinforcement ratios (%)
UB0	34.57	135.01	61.78	6.16	4.11	2.19	1.50	100.00	100.00	2.13
UCB1	37.47	143.77	60.61	5.87	3.77	2.37	1.56	108.56	103.84	
UCB2	28.64	129.04	35.77	5.52	2.83	3.61	1.95	165.07	129.91	
UCB3	72.35	616.85	243.92	13.49	8.03	2.53	1.68	115.73	112.05	
UCB4	40.37	458.56	74.19	11.30	4.13	6.18	2.73	282.84	182.33	
UCB5	42.72	354.37	106.82	11.39	5.46	3.32	2.09	151.83	139.30	
UCB6	36.49	432.43	72.93	11.72	4.71	5.93	2.49	271.36	166.13	
UCB7	39.49	441.40	62.98	11.49	3.65	7.01	3.14	320.72	209.74	

- OCB Series:

The ductility of eight reinforced concrete beams was analyzed relatively to OB0 served as the reference specimen with a μ_E 11.08 and a μ_Δ of 4.34. All beams exhibited reductions in ductility Table 11. OCB1 showed a significant decrease of 70.9% in μ_E and 52.3% in μ_Δ, while OCB2 recorded a 59.3% reduction in μ_E and a 44.7% drop in μ_Δ. OCB3 displayed the lowest energy-based ductility, with a 74.5% decrease from OB0, and a 60.1% reduction in displacement-based ductility. OCB4 and OCB5 exhibited moderate ductility values, with μ_E decreases of 66.0% and 41.9%, respectively, and μ_Δ reductions of 51.2% and 30.4%. OCB6 retained more of the original ductility, with a 60.6% drop in μ_E and 45.6% in μ_Δ. Finally, OCB7 showed the smallest relative decline among all specimens, with μ_E and μ_Δ reductions of 66.9% and 48.2%, respectively. These results indicate that OB0 demonstrated superior energy absorption and deformation capacity, and all strengthened beams experienced varying degrees of ductility loss, which is attributed to stiffness increase and failure by shear.

Table 11. Ductility for all OCB beams

Specimen	Max elastic load (KN)	Energy E_u	Energy E_y	Δ_u (mm)	Δ_y (mm)	μ_E	μ_Δ	μ_E Gain ratio	μ_Δ Gain ratio	Steel reinforcement ratios (%)
OB0	46.3	718.92	64.86	13.21	3.04	11.08	4.34	100.00	100.00	
OCB1	73.85	886.10	275.36	14.81	7.16	3.22	2.07	29.03	47.64	
OCB2	63	632.66	140.42	10.95	4.56	4.51	2.40	40.65	55.36	
OCB3	86	752.60	266.61	11.66	6.73	2.82	1.73	25.47	39.95	2.29
OCB4	73	788.18	209.11	13.59	6.41	3.77	2.12	34.01	48.88	
OCB5	41.27	512.63	79.70	11.46	3.79	6.43	3.02	58.03	69.65	
OCB6	54	510.75	117.21	10.03	4.25	4.36	2.36	39.31	54.38	
OCB7	63	559.66	153.05	10.89	4.85	3.66	2.25	32.99	51.74	

- UGB Series:

The reference beam UB0 exhibited values of μ_E = 2.19 and μ_Δ = 1.50. Beam UGB1 demonstrated the most significant improvement, with a μ_E of 7.44 (239.3%) and μ_Δ of 3.00 (100.0%), indicating exceptional energy absorption and deformation capacity Table 12. Similarly, UGB5 outperformed all other specimens in terms of ductility, with a μ_E of 9.74 (344.3%) and a μ_Δ of 4.47 (198.0%). Beams UGB2, UGB3, UGB6, and UGB7 also showed notable enhancements in ductility ranging from (49.5%) to (191.4%) in μ_E and (28.0%) to (88.8%) in μ_Δ. Conversely, UGB4 exhibited a slight decrease in energy-based ductility (2.7%) but maintained a comparable μ_Δ (1.3%), suggesting nearly elastic behavior. These results demonstrate that the type of strengthening and configuration used in UGB1 through UGB8 significantly influenced both the energy dissipation capacity and post-yield deformation, with certain configurations enhancing ductility [72] by more than threefold compared to the un-strengthened reference beam UB 0.

Table 12. Ductility for all UGB beams

Specimen	Max elastic load (KN)	Energy E_u	Energy E_y	Δ_u (mm)	Δ_y (mm)	μ_E	μ_Δ	μ_E Gain ratio	μ_Δ Gain ratio	Steel reinforcement ratios (%)
UB0	34.57	135.01	61.78	5.35	3.57	2.19	1.50	100	100	
UGB1	35.8	507.70	68.23	13.41	4.47	7.44	3.00	340.54	200.12	
UGB2	42	285.11	85.47	9.26	4.83	3.34	1.92	152.66	127.98	
UGB3	58	547.58	167.65	12.78	6.48	3.27	1.97	149.47	131.47	
UGB4	63.68	501.89	235.50	12.74	8.39	2.13	1.52	97.53	101.29	2.13
UGB5	35	624.21	64.12	18.09	4.04	9.74	4.47	445.53	298.25	
UGB6	38.3	353.90	75.54	10.55	4.55	4.68	2.32	214.40	154.77	
UGB7	36.36	402.47	63.21	11.29	3.99	6.37	2.83	291.38	188.88	
UGB8	53	415.30	128.50	10.48	5.80	3.23	1.81	147.90	120.52	

OGB Series:

Beam OB0, with μ_E = 11.08 and μ_Δ = 4.34, served as the reference for comparison. All other beams exhibited reduced ductility values relative to OB0 Table 13. Specifically, OGB2 and OGB4 showed the most significant reductions, with μ_E decreasing by approximately 80% and 73.16%, and μ_Δ by 63.87% and 58.9%, respectively. These results suggest a marked loss in both energy absorption capacity and deformation ability. Moderate reductions were observed in beams OGB1, OGB3, OGB5, and OGB8 with μ_E values reduced by 65.91%, 70.98%, 53.27%, and 50.57% and μ_Δ by 52.11%, 56.13%, 38.92% and 34.43% respectively. Beams OGB6 and OGB7 demonstrated relatively better performance, maintaining μ_E values at 87.78% and 60.32% of OB0, and μ_Δ values at 92.95% and 69.11%, indicating enhanced residual ductility compared to the other specimens. Overall, the results confirm that OGB6 exhibits the highest ductile behavior among the tested beams even if it's a decrease but succeeded to restore the ductility, and highlight that in deep beams subjected to shear failure, 45° with anchorage configuration is the best solution to recover ductility.

From a practical perspective, the investigated FRP systems should be considered alongside conventional strengthening solutions such as steel jacketing and alternative composite systems such as basalt-fiber-reinforced polymers (BFRP). Steel jacketing can provide substantial strength and confinement but introduces additional weight, corrosion-related concerns, and more demanding installation procedures. FRP systems, in contrast, offer lightweight and corrosion-resistant strengthening with relatively simple installation and the possibility of targeting specific deficient regions. Within FRP-based solutions, CFRP provides high mechanical efficiency and stiffness, whereas GFRP offers a more economical alternative with greater deformability. BFRP represents another promising alternative, particularly where durability and cost are important considerations, although its application to shear-critical deep members remain less extensively documented.

Unlike studies focused primarily on flexural strengthening, the present investigation addresses the coupled flexural–shear response of deep T-beams, with particular emphasis on the control of diagonal cracking and the prevention of premature shear failure. Consequently, the value of the proposed FRP systems extends beyond a simple comparison of material efficiency. Their practical significance lies in their potential to provide an integrated strengthening solution capable of improving both flexural performance and shear resistance within a single intervention. The present results therefore provide useful evidence for identifying FRP configurations that can serve as viable alternatives to more invasive conventional methods, while balancing load-carrying capacity, ductility, stiffness, constructability, durability, and economy. Importantly, for the deep T-beams investigated herein, the strengthening material alone is not sufficient; the configuration, anchorage, and ability to control shear cracking remain decisive factors in achieving the desired structural performance.

Table 13. Ductility for all OGB beams

Specimen	Max elastic load (KN)	Energy E_u	Energy E_y	Δ_u (mm)	Δ_y (mm)	μ_E	μ_Δ	μ_E Gain ratio	μ_Δ Gain ratio	Steel reinforcement ratios (%)
OB0	46.3	718.92	64.86	15.19	3.50	11.08	4.34	100	100	
OGB1	65	649.10	171.81	12.71	6.11	3.78	2.08	34.08	47.89	
OGB2	68	417.97	188.71	10.05	6.41	2.21	1.57	19.98	36.13	
OGB3	75	650.75	202.28	12.44	6.53	3.22	1.90	29.02	43.86	
OGB4	65	418.27	140.62	8.95	5.02	2.97	1.78	26.84	41.10	2.29
OGB5	52.42	587.75	113.47	12.94	4.88	5.18	2.65	46.73	61.08	
OGB6	50.73	810.10	83.26	16.13	4.00	9.73	4.03	87.78	92.95	
OGB7	43.91	540.24	80.80	13.24	4.41	6.69	3.00	60.32	69.11	
OGB8	56.65	685.93	125.19	14.51	5.10	5.48	2.85	49.43	65.57	

5. Failure Modes of All Series

All tested beam specimens exhibited a shear-dominated failure mode. Initially, a single crack developed near the support and propagated diagonally at approximately 45° toward the loading point. As the applied load increased, the crack gradually widened, indicating progressive shear damage. Among the different reinforcement configurations, the specimen strengthened with a 45° fiber orientation combined with anchorage showed the most effective crack control, significantly slowing the propagation of shear cracks. At ultimate load, shear cracks became fully developed, accompanied by concrete crushing in the compression zone, leading to final peak failure.

The effect of FRP orientation is closely related to the shear-transfer mechanism governing the response of the tested deep T-beams. In shear-critical members, diagonal cracking develops along trajectories associated with the principal tensile stresses, while the compression strut transfers the corresponding compressive stresses toward the supports. Consequently, the effectiveness of an FRP strengthening system depends not only on its mechanical properties but also on its ability to interact with these principal stress paths and intercept the developing diagonal cracks.

The 0° longitudinal reinforcement primarily contributes to the flexural response and restrains longitudinal crack development. However, because its fibers are oriented parallel to the beam axis, its direct contribution to controlling diagonal shear cracks is limited. In contrast, the ±45° orientation provides a more favorable alignment with the diagonal cracking pattern. The inclined fibers cross the developing shear cracks and can therefore transfer tensile stresses across the cracked region, restrain crack opening and propagation, and promote a more distributed stress-transfer mechanism. This effect becomes particularly significant for the U-shaped ±45° configuration. By extending the strengthening around the web, the U-wrap provides a continuous load-transfer path across the critical shear region and improves the interaction between the FRP and the concrete substrate. The inclined fibers intersect the diagonal cracks over their development path, while the U-shaped arrangement helps transfer the induced tensile forces into the surrounding concrete and toward the compression region. This combined action delays the propagation of critical diagonal cracks and reduces the likelihood of premature localized shear failure. As a result, the FRP can remain engaged over a greater portion of the loading history, leading to higher load-carrying capacity and improved deformation performance. The superior response of the inclined U-wrap should therefore not be attributed solely to the higher mechanical properties of the FRP material. Rather, it results from the compatibility between the strengthening orientation and the internal stress field of the shear-critical beam. The experimental results consequently demonstrate that, for deep RC T-beams, the orientation and continuity of the strengthening system can be as important as the FRP material itself, because an appropriately oriented system can more effectively intercept diagonal cracking and redistribute stresses within the critical shear zone.

6. Flexural Stiffness Variation Under Increasing Load

In a four-point bending test of a reinforced concrete (RC) beam, the flexural rigidity EI can be determined by analyzing the load-deflection behavior using Macaulay's method. To derive EI, Macaulay's brackets are employed to express the bending moment distribution M(x) as a piecewise function, accurately capturing the internal force variations along the beam's span. By applying the fundamental relationship:

$$EI\frac{d^2y}{dx^2} = M(x) \tag{1}$$

and integrating it twice with respect to x, the deflection profile y(x) is obtained. Appropriate boundary conditions enable the determination of the integration constants. The maximum deflection at mid-span is given by the expression:

$$\delta_{max} = \frac{23.F_i.a^3}{24.EI} \tag{2}$$

which, upon rearrangement, allows the calculation of EI as a function of the applied load Fi, geometric parameters, and the measured deflection using the formula from strength of materials theory:

$$\delta_{max} = 1.15 * \delta_F \tag{3}$$

with δ_F representing the displacement at the point of application of the force.

The mechanical response of a reinforced concrete (RC) beam evolves progressively with increasing load, and its stiffness is therefore not necessarily constant throughout the loading history. In the initial uncracked stage, the concrete section contributes to both compression and tension, and the flexural rigidity can be reasonably represented by the gross-section value, (EI_g). With increasing load, tensile cracking progressively reduces the contribution of concrete in tension, resulting in a reduction in the effective flexural stiffness. At higher load levels, the response becomes increasingly nonlinear due to crack propagation, redistribution of internal forces, and, where applicable, inelastic deformation of the reinforcement. Consequently, the stiffness derived from a global force–displacement response should be interpreted in relation to the actual deformation mechanisms governing each stage of loading.

For the present experimental investigation, particular attention is required because the tested members are deep T-beams with a low shear span-to-effective depth ratio (a/d=2.22) and predominantly shear-controlled failure. Accordingly, the measured mid-span displacement cannot be considered exclusively as a flexural deformation; it may include significant contributions from shear deformation, particularly following the development of diagonal shear cracking. Therefore, the stiffness calculated from the measured force–displacement response is interpreted herein as an equivalent or apparent stiffness, rather than as a pure flexural rigidity.

The gross-section rigidity, EI_g, is consequently considered only as a theoretical reference corresponding to the uncracked condition. In contrast, the stiffness calculated at each load level, EI, is allowed to vary with the applied load and is used to characterize the global structural response. The resulting EI = f(Fi) curves therefore provide a comparative indicator of the stiffness evolution of the different beam configurations rather than a direct measurement of the intrinsic flexural rigidity of the section. This distinction is particularly important for the present shear-dominated specimens. An apparent reduction in EI should not be attributed exclusively to flexural cracking, since the progressive development of diagonal shear cracks can increase shear deformation and consequently reduce the global load displacement stiffness. Similarly, variations observed at very low load levels may partly reflect the sensitivity of the calculated stiffness to small measured displacements, as well as initial seating and alignment effects within the experimental setup. The evolution of EI should therefore be understood as the combined manifestation of flexural response, shear deformation, cracking, and experimental effects.

Accordingly, the EI = f(Fi) representation adopted in this study is intended primarily to capture and compare the evolution of the global stiffness among the investigated strengthening configurations. This approach provides a useful engineering indicator of how CFRP and GFRP strengthening modify the structural response while avoiding the assumption that a single constant EI can fully describe the behavior of a shear-critical deep beam. The interpretation is thus consistent with the governing failure mechanism and provides a more physically meaningful assessment of stiffness than treating EI as a constant material or sectional property throughout the loading process.

When analyzing the EI = f(Fi) curve obtained for a reinforced concrete beam, several characteristic phases of structural behavior can be identified. In the first phase, the initial rise of EI appears curved and nonlinear Fig. 8. This nonlinearity can be attributed to play within the experimental setup, such as progressive contact between the beam and the supports or loading devices. It may also reflect intrinsic material behavior, particularly the fact that concrete is not perfectly elastic under very low loads, with early microcracking or initial nonlinearities.

In the second phase, a continuous increase in EI is observed Fig. 9, which might seem counterintuitive. However, this evolution is understandable: as long as the beam remains uncracked, the concrete in tension continues to fully contribute to the global stiffness. Additionally, as the load is applied, the test setup tends to realign itself, reducing parasitic effects due to friction or sliding at interfaces. From an analytical point of view, the calculation of EI from $EI = \frac{M}{\phi}$ shows that for very small initial curvatures, the apparent stiffness can be notably high. This stage concludes with a reduction in rigidity, marking the point of maximum elastic load.

Finally, the third phase is characterized by a decrease in EI over two distinct stages Fig. 10, Fig. 11. The first drop corresponds to the appearance of the first cracks in the constant moment region; the loss of stiffness is related to the cracking of concrete in tension, which can no longer fulfill its structural role. During the second stage, the stiffness continues to decline more significantly, indicating either the propagation of cracks or the yielding of the steel reinforcement. This phase may also be accompanied by localized plasticity of the steel or creep phenomena, signaling the approach of the ultimate limit state.

In conclusion, the particular shape of the curve reveals a complex and progressive behavior of the beam before and after cracking. It highlights the importance of a detailed analysis of initial setup imperfections, progressive alignment, distributed cracking, and the redistribution of stresses between concrete and reinforcement. These observations reflect a structured loss of stiffness, typical of a well-instrumented beam subjected to a rigorous experimental protocol.

UCB Series:

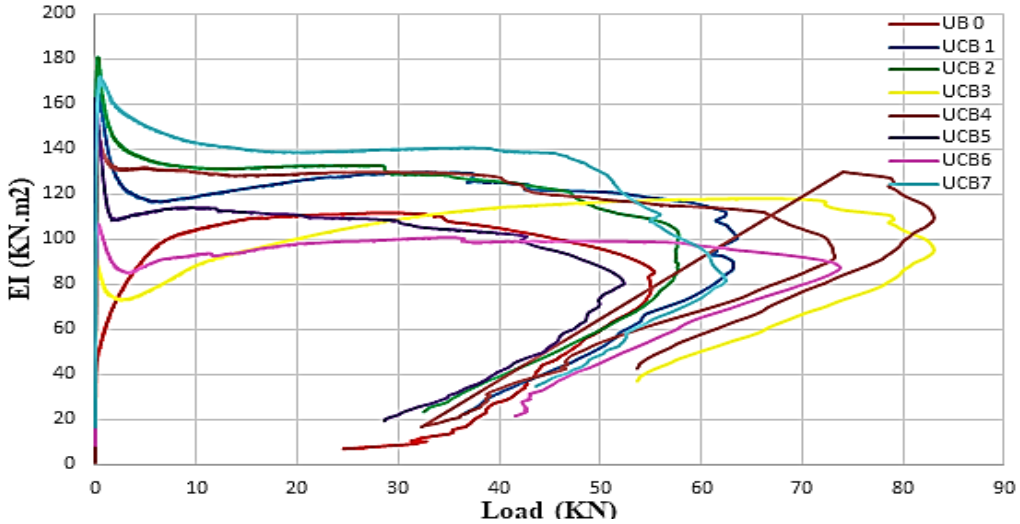


Fig. 8. Flexural stiffness variation under increasing load for UCB series

OCB Series:

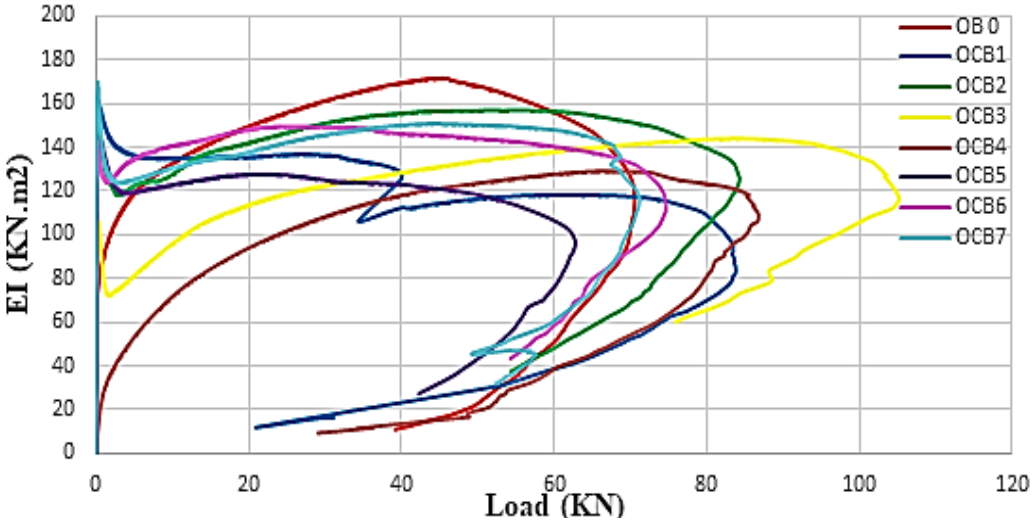


Fig. 9. Flexural stiffness variation under increasing load for OCB series

UGB Series:

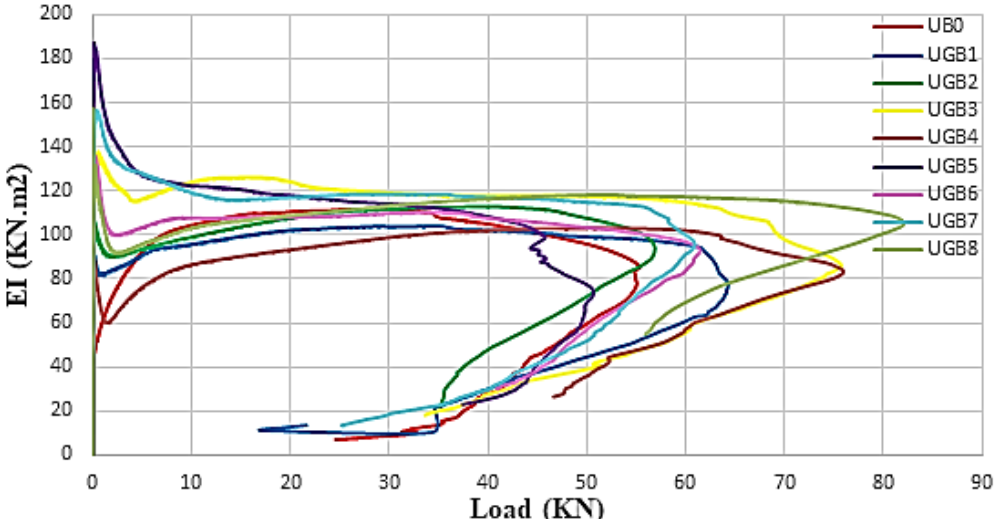


Fig. 10. Flexural stiffness variation under increasing load for UGB series

OGB Series:

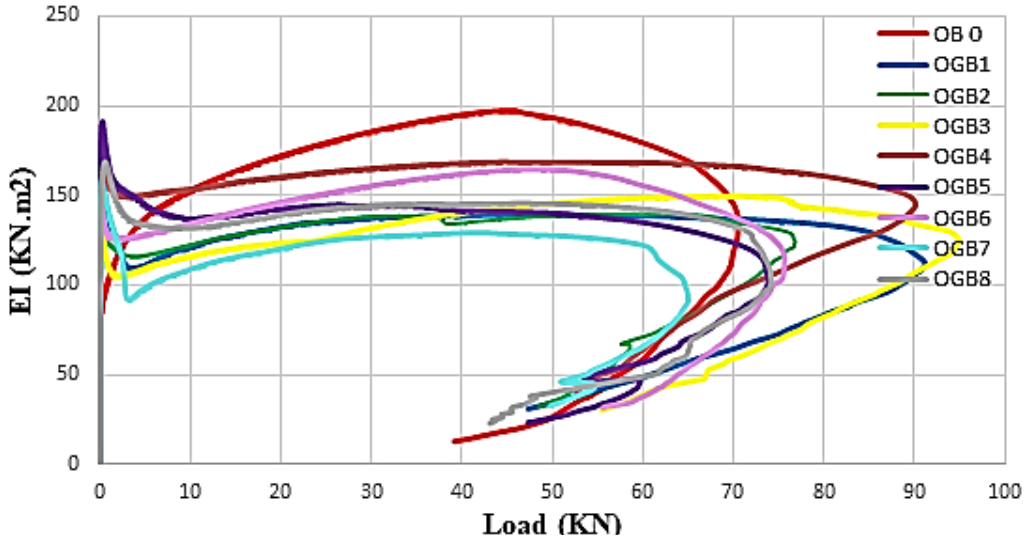


Fig. 11. Flexural stiffness variation under increasing load for OGB series

7. Conclusions

- The experimental results showed that the tested T-shaped RC beams exhibited predominantly shear-controlled failure, characterized by the development and propagation of diagonal cracks in the shear spans. This behavior confirms that, for the investigated deep-beam geometry (a/d=2.2), flexural FRP strengthening alone cannot prevent premature shear failure when shear governs the structural response.
- Among the investigated strengthening configurations, the 45° U-shaped FRP arrangement provided the most favorable overall response. The experimental force displacement curves showed improved load-carrying capacity and deformation performance compared with the corresponding configurations without inclined shear strengthening. The observed diagonal cracking also indicated that the inclined fibers were more effectively positioned to intersect the principal shear cracks.
- The results demonstrate that the relatively low-strength concrete substrate can limit the mobilization of the FRP strengthening system when premature shear failure occurs. The effectiveness of FRP strengthening should therefore be considered in conjunction with the mechanical quality of the concrete substrate. Increasing the mechanical capacity of the substrate is expected to improve stress transfer and allow a greater contribution from the FRP system; however, this effect requires dedicated experimental investigation using different concrete strength levels. The relatively low concrete compressive strength is relevant to the assessment of strengthening efficiency because the concrete substrate plays a fundamental role in transferring stresses to the externally applied FRP reinforcement. A mechanically weak substrate may experience premature cracking or shear failure before the full tensile capacity of the FRP can be mobilized. Consequently, the measured strengthening efficiency reflects not only the properties and configuration of the FRP system but also its interaction with the concrete substrate.
- The reinforcement ratio had a clear influence on the force displacement response and ductility of the tested beams. The under-reinforced configurations generally exhibited greater deformation capacity, whereas the over-reinforced configurations showed a stiffer response and reduced ductility. For the investigated over-reinforced beams, the addition of the 45° U-shaped FRP configuration with appropriate anchorage improved the deformation capacity, demonstrating its potential to mitigate the loss of ductility associated with increased reinforcement ratios.
- A difference in deformation behavior was observed between the CFRP and GFRP strengthened beams. The GFRP configurations generally exhibited greater deformation capacity, while the CFRP configurations provided higher stiffness and load-carrying capacity

within the tested configurations. Accordingly, GFRP may be considered when deformation capacity is prioritized, whereas CFRP is more appropriate when higher stiffness and load capacity are the primary objectives.

- The experimental results indicate that strengthening selection should be based on the governing structural deficiency rather than on flexural capacity alone. For the shear-critical beams investigated in this study, combining flexural reinforcement with an appropriately anchored shear-strengthening configuration provided a more effective structural response than relying on flexural strengthening alone.
- The investigated Woven Roving E300 and rolled-FRP NSM configurations demonstrated promising strengthening potential within the tested experimental conditions. Their measured force displacement responses provide a quantitative basis for further investigation of these systems as alternative strengthening solutions. However, their applicability to full-scale structures requires additional validation, particularly regarding anchorage, durability, bond behavior, and variability in concrete mechanical properties.
- The present results provide a sound experimental basis for selecting and applying FRP strengthening systems in shear-critical RC T-beams under the investigated conditions. The identified strengthening mechanisms and quantitative performance indicators enable direct comparison of strengthening configurations. The applicability of these findings to different concrete strengths, shear span-to-depth ratios, anchorage arrangements, and structural scales requires further experimental validation, while numerical modelling can extend the observed trends and support refined engineering design approaches.
- Future research should focus on integrated strengthening approaches that address both flexural and shear deficiencies in shear-critical RC beams. Particular emphasis should be placed on optimizing NSM reinforcement configurations, anchorage systems, and hybrid strengthening schemes combining NSM reinforcement with inclined U-shaped CFRP/GFRP wraps. Advanced numerical simulations using ABAQUS are being prepared to assess force displacement behavior, structural ductility, failure mechanisms, and the response under varying shear span-to-depth ratios. The quantitative experimental results obtained in this study provide a valuable benchmark for assessing existing FRP design provisions and refining shear-strength and deformation models, thereby supporting the development of more reliable design approaches for structural rehabilitation.

References

[1] Askar MK, et al. Flexural and shear strengthening of reinforced concrete beams using FRP composites: A state of the art. Case Studies in Construction Materials. 2022;17. https://doi.org/10.1016/j.cscm.2022.e01189

[2] Jahami A, et al. An Updated Review on the Effect of CFRP on Flexural Performance of Reinforced Concrete Beams. International Journal of Concrete Structures and Materials. 2024;18. https://doi.org/10.1186/s40069-023-00651-y

[3] Zombré W. Durability of Composite Materials in a Civil Engineering Environment: Multi-Scale Experimentation and Statistical Analysis. Doctoral School No. 162 (Mechanics, Energetics, Civil Engineering, Acoustics); 2019.

[4] Milan Z. Introduction to Seismic Construction. Le Moniteur; 2019.

[5] Mahdi V. Experimental Investigation on Flexural Capacity of Reinforced Concrete Beams Strengthened with 3D-Fiberglass, CFRP and GFRP. International Journal of Concrete Structures and Materials. 2022;16. https://doi.org/10.1186/s40069-022-00508-w

[6] Jaafar A, et al. Study The Behavior of Square Reinforced Concrete Columns Strengthened with CFRP. Electronic Journal of Structural Engineering (EJSE). 2023;23:79-84. https://doi.org/10.56748/ejse.23487

[7] Wei B, et al. Research on the flexural behavior of polypropylene fiber reinforced concrete beams with hybrid reinforcement of GFRP and steel bars. Materials and Structures. 2024;57. https://doi.org/10.1617/s11527-024-02343-9

[8] Manfredi V, et al. Seismic strengthening and energy efficiency: Towards an integrated approach for the rehabilitation of existing RC buildings. Buildings. 2018;8(13). https://doi.org/10.3390/buildings8030036

[9] Kassoul A. REHABILITATION OF REINFORCED CONCRETE STRUCTURES. [Performance]; 2014.

[10] Milan Z. Seismic Construction Treatise. Parentheses; 2004.

[11] Fardis, et al. FRP-Encased Concrete as a Structural Material. Magazine of Concrete Research. 1982;34. https://doi.org/10.1680/macr.1982.34.121.191
[12] Fardis, et al. Concrete Encased in Fiberglass-Reinforced Plastic. ACI Journal Proceedings. 1981;78. https://doi.org/10.14359/10527
[13] Al-Nsour R, et al. Flexural repairing of heat damaged reinforced concrete beams using. Composites Part C: Open Access. 2023;12. https://doi.org/10.1016/j.jcomc.2023.100404
[14] Zapris AG, et al. Novel approach for strengthening T-beams deficient in shear with. Developments in the Built Environment. 2024;18. https://doi.org/10.1016/j.dibe.2024.100394
[15] Zapris AG, et al. Fiber Reinforced Polymer Debonding Failure Identification. Polymers. 2023;15. https://doi.org/10.3390/polym15020278
[16] Saribiyik A, et al. Experimental study on shear strengthening of RC beams with basalt FRP strips using different wrapping methods. Engineering Science and Technology. 2020;24. https://doi.org/10.1016/j.jestch.2020.06.003
[17] Hemida OAR, et al. Flexural Behaviour of Recycled Reinforced Concrete Beams Strengthened/ Repaired with CFRP Laminates. Journal of Engineering and Applied Science. 2023;70. https://doi.org/10.1186/s44147-023-00235-3
[18] Sengun K, et al. Performance of RC Beams Strengthened in Flexure and Shear with CFRP and GFRP. Iranian Journal of Science and Technology. 2023;48. https://doi.org/10.1007/s40996-023-01305-5
[19] Zakkaria MFM, et al. Flexural behavior of fiber-reinforced concrete beams with GFRP rebars under marine environmental conditions. The International Journal of Advanced Manufacturing Technology. 2023. https://doi.org/10.1007/s00170-023-12690-6
[20] Arslan MH, et al. Shear strengthening of reinforced concrete T-beams with anchored and non-anchored CFRP fabrics. Structures. 2022;39. https://doi.org/10.1016/j.istruc.2022.03.046
[21] Ashteyat A, et al. The behavior of strengthened RC beams under pure torsion using NSM-CFRP rope. International Journal of Building Pathology and Adaptation. 2024;43:1577-1594. https://doi.org/10.1108/IJBPA-02-2023-0024
[22] Kaliyappan SP, et al. Behavior of reinforced concrete beam with CFRP and GFRP laminates. Matéria (Rio J.). 2023;28. https://doi.org/10.1590/1517-7076-rmat-2023-0222
[23] Ou Y, et al. Mechanical Characterization of the Tensile Properties of Glass Fiber and Its Reinforced Polymer (GFRP) Composite under Varying Strain Rates and Temperatures. 2016;8. https://doi.org/10.3390/polym8050196
[24] Montaser WM. Structural Behaviour of Polystyrene Foam Lightweight Concrete Beams Strengthened with FRP Laminates. International Journal of Concrete Structures and Materials. 2022;16. https://doi.org/10.1186/s40069-022-00549-1
[25] Yang J, et al. Experimental study of FRP-strengthened concrete beams with corroded reinforcement. Construction and Building Materials. 2021;301. https://doi.org/10.1016/j.conbuildmat.2021.124076
[26] Soudki K, et al. Behavior of CFRP Strengthened Reinforced Concrete Beams in Corrosive Environment. Journal of Composites for Construction. 2007;11. https://doi.org/10.1061/(ASCE)1090-0268(2007)11:3(291
[27] Jaham A, et al. An Updated Review on the Effect of CFRP on Flexural Performance of Reinforced Concrete Beams. International Journal of Concrete Structures and Materials. 2024;18. https://doi.org/10.1186/s40069-023-00651-y
[28] Mohamed OA. Numerical Analysis of Reinforced Concrete Beam Strengthened with CFRP or GFRP Laminates. Key Engineering Materials. 2016;707. https://doi.org/10.4028/www.scientific.net/KEM.707.51
[29] Zhang Z, et al. Shear Strengthening of Reinforced Concrete Beams Using Carbon-Fiber-Reinforced Polymer Laminates. Journal of Composites for Construction. 2005;9. https://doi.org/10.1061/(ASCE)1090-0268(2005)9:2(158
[30] Hosen MA, et al. Flexural Performance of RC Beams Strengthened with. Materials. 2021;14. https://doi.org/10.3390/ma14112809
[31] Hosen MA, et al. Behavior and modeling of RC beams strengthened with NSM-steel technique. Structural Engineering and Mechanics. 2023;88:67-81. https://doi.org/10.1016/j.prostr.2023.10.072
[32] Hosen MA, et al. Glass Fiber Reinforced Polymer (GFRP) Bars for Enhancing the Flexural Performance of RC Beams Using Side-NSM Technique. Polymers. 2017;9(5):180. https://doi.org/10.3390/polym9050180
[33] Shukri AA, et al. Behaviour of precracked RC beams strengthened using the side-NSM technique. Construction and Building Materials. 2016;123:617-626. https://doi.org/10.1016/j.conbuildmat.2016.07.066
[34] Hosen MA, et al. Near Surface Mounted Composites for Flexural Strengthening of Reinforced Concrete Beams. Polymers. 2013;8. https://doi.org/10.3390/polym8030067

[35] Hosen MA, et al. Eliminating concrete cover separation of NSM strengthened beams by CFRP end anchorage. Structural Engineering and Mechanics. 2015;56:899-916. https://doi.org/10.12989/sem.2015.56.6.899
[36] Hosen MA, et al. Side-NSM composite technique for flexural strengthening of RC beams. Computers and Concrete. 2017;20:439-448.
[37] Altunişik AC, et al. Field Observations and Damage Evaluation in Reinforced Concrete Buildings After the February 6th, 2023, Kahramanmaras-Turkiye Earthquakes. Journal of Earthquake and Tsunami. 2023;17.
[38] Aung WY, et al. Damage mechanisms and seismic vulnerability of building structures following the 2025 M 7.7 Mandalay earthquake sequence, Myanmar. Engineering Failure Analysis. 2025;180. https://doi.org/10.1016/j.engfailanal.2025.109849
[39] Bilgin H, et al. Reflections from the 2019 Durrës Earthquakes: An Earthquake Engineering Evaluation for Masonry Typologies. Buildings. 2023;13. https://doi.org/10.3390/buildings13092227
[40] Peker FÜ, et al. Seismic performance assessment and strengthening of a residential RC building damaged in the 2023 Türkiye Earthquakes: A case study. Scientific Reports. 2026;16:24. https://doi.org/10.1038/s41598-026-53823-7
[41] Avcil F, et al. Effects of Transverse Reinforcement Detailing on the Damage Mechanisms of RC Elements: Lessons from the 2023 Kahramanmaraş Earthquakes. Buildings. 2026;16. https://doi.org/10.3390/buildings16142897
[42] Hosen MA, et al. Inclusion of CFRP-Epoxy Composite for End Anchorage in NSM Strengthened Beams. Advances in Materials Science and Engineering. 2015. https://doi.org/10.1155/2015/812797
[43] Hosen MA, et al. Potential Side-NSM Strengthening Approach to Enhance the Flexural Performance of RC Beams. Structural Engineering and Mechanics. 2023;85:179-195.
[44] Işık E, et al. Enhancing the seismic safety of upgraded RC buildings using FRP retrofitting: analytical and field evidence from the 2023 Kahramanmaraş earthquakes. Bulletin of Earthquake Engineering. 2025;24. https://doi.org/10.1007/s10518-025-02338-z
[45] Işık E. Strengthening strategies for mitigating damage induced by high ground stories: field data and analytical findings from RC buildings in the kahramanmaraş earthquakes. Bulletin of Earthquake Engineering. 2026. https://doi.org/10.21203/rs.3.rs-9601642/v1
[46] Issa S, et al. Shear Strengthening and Repairing of Reinforced Concrete T-Beam Exposed to high Temperature Using Near Surface Mounted Carbon Fiber Reinforced Polymers Ropes. Engineered Science. 2024;31(1872).
[47] Sika El Djazair SPA. Product data sheet SikaWrap®-230 C. 2023.
[48] VISA COMPOSITES. Product data sheet EWR300-W612.
[49] Sika El Djazair SPA. Product data sheet Sikadur®-330. 2023.
[50] Truong BT. Formulation, mechanical performance, and applications of a TRC material for strengthening and repairing concrete and reinforced concrete structures: Experimental and numerical approaches. University of Lyon; 2016.
[51] Chbani, et al. Formulation of Ordinary Concrete using the Dreux-Gorisse Method. Procedia Structural Integrity. 2020;28:430-439. https://doi.org/10.1016/j.prostr.2020.10.050
[52] McCain KA. The Effect of Scale on the Resistance of Reinforced Concrete Beams to Shear. Purdue University; 2013.
[53] MTS. Available from: https://www.mts.com.
[54] Attari, et al. Efficiency of strengthening concrete beams using FRP. 2012.
[55] Si Youcef Y, et al. CFRP confinement effectiveness on the behavior of reinforced concrete columns with respect to buckling instability. Construction and Building Materials. 2015;48:35-51. https://doi.org/10.1016/j.conbuildmat.2015.02.006
[56] Zhang HZ. Performance of Deep Beams with Topologically Optimized Reinforcements: Experimental Verification and Comparison. Structural Engineering. 2025;151:04024015. https://doi.org/10.1061/JSENDH.STENG-13495
[57] Wardeh G, et al. Shear strength of reinforced concrete beams with recycled aggregates. Engineering Structures. 2019. https://doi.org/10.1177/1369433219829815
[58] Kani G. The Riddle of Shear Failure and Its Solution. Journal Proceedings. 1964;61:441-468. https://doi.org/10.14359/7791
[59] Chalioris CE, et al. Application of a Reinforced Self-Compacting Concrete Jacket in Damaged Reinforced Concrete Beams under Monotonic and Repeated Loading. Journal of Engineering. 2012;2013. https://doi.org/10.1155/2013/912983
[60] Hu B, et al. Effect of shear span-to-depth ratio on shear strength components of RC beams. Engineering Structures. 2018;168:770-783. https://doi.org/10.1016/j.engstruct.2018.05.017
[61] Fenwick, et al. The Behavior of Reinforced Concrete Beams in Shear. Proceedings of the New Zealand Society for Earthquake Engineering. 1972;5.

[62] Zararis P. Shear Compression Failure in Reinforced Concrete Deep Beams. Journal of Structural Engineering. 2003;129. https://doi.org/10.1061/(ASCE)0733-9445(2003)129:4(544
[63] Alav DS, et al. Shear strengthening of sub-standard reinforced concrete beams with CFRP: Influence of fiber areal weight, wrap scheme and concrete strength. Structures. 2025;82. https://doi.org/10.1016/j.istruc.2025.110734
[64] El-Shafiey TF, et al. Behavior of strengthened RC beams using different techniques under static loading. International Conference on Advances in Structural and Geotechnical Engineering (ICASGE'17); 2017.
[65] Pour AK, et al. Enhancing Flexural Strength of RC Beams with Different Steel-Glass Fiber-Reinforced Polymer Composite Laminate Configurations: Experimental and Analytical Approach. Infrastructures. 2024;9. https://doi.org/10.3390/infrastructures9040073
[66] Renić T, et al. Ductility of Concrete Beams Reinforced with FRP Rebars. Buildings. 2021;11. https://doi.org/10.3390/buildings11090424
[67] Cao VV. Effects of CFRP U-Wraps on the Behavior of NSM GFRP Retrofitted Reinforced Concrete Beams. Journal of Composites for Construction. 2025;29. https://doi.org/10.1061/JCCOF2.CCENG-4884
[68] Lu ZH, et al. Shear behavior degradation and failure pattern of reinforced concrete beam with chloride-induced stirrup corrosion. Advances in Structural Engineering. 2019;22. https://doi.org/10.1177/1369433219855917
[69] Zhang M, et al. Experimental Study on the Shear Behavior of Reinforced Highly Ductile Fiber-Reinforced Concrete Beams with Stirrups. Buildings. 2022;12. https://doi.org/10.3390/buildings12081264
[70] Wei B, et al. Finite element analysis of ductility and flexural capacity of FRP and steel bars hybrid reinforced concrete beams. Structural Concrete. 2025;26. https://doi.org/10.1002/suco.202301066
[71] Hose MA, et al. Ductility Enhancement of Sustainable Fibrous-Reinforced High-Strength Lightweight Concrete. Polymers. 2022;14(14). https://doi.org/10.3390/polym14040727
[72] Ozturkoglu O, et al. An Experimental Study on the Effect of GFRP and CFRP Strengthening on the Static and Dynamic Behavior of R/C Beams Under Progressive Damage. Applied Sciences. 2024;14. https://doi.org/10.3390/app14219920
[73] Caprani C. Deflection of Flexural Members - Macaulay's Method. 2009.
[74] Glaisher J. A Note on the Deflection of Beams by W.H. Macaulay (1919). Messenger of Mathematics. 48:129.
[75] Stephen N. Macaulay's Method for a Timoshenko Beam. International Journal of Mechanical Engineering Education. 2007;35:285-292. https://doi.org/10.7227/IJMEE.35.4.3